WORLD CONFERENCE ON TIMBER ENGINEERING 2025
BRISBANE, AUSTRALIA
Advancing Timber for the Future Built Environment

EVALUATING THE SEISMIC PERFORMANCE OF HYBRID REINFORCED CONCRETE FRAMES WITH CLT SHEAR WALLS: EXPERIMENTAL AND ANALYTICAL APPROACHES

Hamood Alwashali[1], Satoshi Kumagawa[2], Chunri Quan[3], Kiwoong Jin[4] , Gary M. Raftery[5]

ABSTRACT: Hybrid building systems, such as integrating Cross-Laminated Timber (CLT) walls into Reinforced Concrete (RC) structures, are gaining attention as a sustainable approach to reducing CO_2 emissions and promoting a carbon-neutral society. Despite its potential, research on the failure mechanisms, seismic capacity, and stiffness evaluation of this hybrid system remains limited. To address this gap, this study investigates the feasibility of using CLT shear walls within RC frames through experimental testing and the development of a practical macro model for structural analysis. Two 1/3-scale RC frame specimens with CLT infill walls were tested under static cyclic loading, utilizing different connection systems—one with shear keys and the other without. The experimental results were used to validate a macro model that represents CLT walls as diagonal braces (axial springs), providing a practical tool for the structural design.

KEYWORDS: Reinforced Concrete Building, CLT walls, Macro model, Hybrid structures

1 – INTRODUCTION

Reinforced concrete (RC) walls are essential structural components in RC buildings, designed to resist lateral forces during seismic events. While effective in earthquake-prone regions, recent earthquakes—such as the 2011 Great East Japan Earthquake—have highlighted the challenges associated with repairing RC walls and quantifying their residual seismic capacity [1]. Similar issues have been observed globally, including in the 2010 Christchurch Earthquake in New Zealand, where 80% of the demolished buildings in Christchurch's Central Business District were RC structures deemed uneconomical to repair [2].

In other instances, earthquakes have caused significant damage to RC buildings with masonry infill walls, as exemplified recently by the 2023 Turkey-Syria Earthquake. Masonry infill walls are generally classified as non-structural elements; however, their interaction with the surrounding frame during seismic events often leads to structural behavior. Due to their brittle nature, they are susceptible to moderate to severe damage, as observed in numerous past earthquakes. This vulnerability has been extensively investigated in various studies, including Alwashali et al.[3].

A potential strategy for improving seismic resilience is to replace RC walls or masonry infill walls with a material that provides sufficient stiffness while being more ductile and easily repairable. In this context, Cross-Laminated Timber (CLT) has emerged as a promising alternative, functioning as an infill shear wall within RC frames. CLT, first developed in Austria in the 1990s, is an engineered wood product that is attracting much attention, with a shear strength of approximately 3 MPa—comparable to that of RC walls.

Integrating CLT walls into RC buildings offers several advantages. CLT is lightweight, provides high strength, enhances lateral stiffness and ductility, and can be efficiently installed in existing RC structures. In the event of earthquake damage, CLT walls can be replaced more easily than traditional RC elements, reducing repair time and costs. Additionally, the use of CLT promotes sustainable construction by lowering carbon emissions. Recognizing these benefits, recent studies have explored its feasibility as shear walls in RC buildings.

[1] Hamood Alwashali, Graduate School of Environmental, Life, Natural Science, & Technology, Okayama University, Okayama, Japan, Hamood@okayama-u.ac.jp

[2] Satoshi Kumagawa, Graduate School of Engineering, Okayama University, Okayama, Japan, pnhz1vy2@s.okayama-u.ac.jp

[3] Chunri Quan, Dept. of Arch., Osaka Institute of Technology, Osaka, Japan, chunri.quan@oit.ac.jp

[4] Kiwoong Jin, Dept. of Architectural Engineering, Hannam University, Daejeon, Korea, jink@hnu.kr

[5] Gary M. Raftery, Dept. of Civil and Environmental Engineering., Faculty of Eng., University of Auckland, Auckland, New Zealand, g.raftery@auckland.ac.nz

https://doi.org/10.52202/080513-0105

Several experimental studies have investigated the performance of RC frames with CLT infill. Haba et al. [4] tested five 1/3-scale RC frames with different CLT infill types, focusing on shear failure mechanisms in older seismic designs. Stazi et al. [5] analyzed the interaction between CLT infill and RC frames through experimental and numerical approaches. More recently, Smiroldo et al. [6] and Too et al. [7] examined various CLT-RC connection details through experimental testing.

Despite these efforts, research on CLT-RC hybrid systems remains limited. The failure mechanisms, strength capacity, and stiffness characteristics are not yet fully understood, as highlighted in a previous study by the authors [8]. Moreover, practical analytical models for accurately simulating their behavior are still lacking, presenting a challenge for widespread implementation.

To address this gap, this study investigates the seismic performance of CLT shear walls integrated into RC frames through experimental testing. Two 1/3-scale RC frame specimens with CLT infill walls were tested under static cyclic loading. The primary parameter examined is the effect of different connection systems between the RC frame and CLT wall—one utilizing shear keys and the other without. A simplified macro model for the system is proposed and validated against experimental results.

2 – EXPERIMENTAL PROGRAM

2.1 Design of specimens

The study involves testing two 1/3 scaled specimens of RC frame with CLT infill wall as shown in Fig.1. The main parameter differentiating the tests is the presence or absence of shear keys between the RC frame and the CLT wall.

Specifically, Specimen S-SE was designed with two shear keys (each of dimensions: 100 × 200 × 200 mm in height × length × thickness) in the RC frame on the upper and lower beams. These shear keys are thought to ensure the proper transfer of shear forces between the RC frame and the CLT wall, in addition to the epoxy, as shown in Fig. 1 (a). The shear key contained 6D16 bars and designed to withstand the forces from the CLT wall. Specimen S-E was designed with only epoxy filled between CLT panels and RC, as shown in Fig. 1 (b).

The RC beams were designed with a higher capacity than the columns to reflect real-world conditions, particularly in older buildings. Consequently, the RC frame was expected to develop its ultimate flexural capacity, with plastic hinges forming at the column ends. Both specimens incorporated a CLT panel measuring 992 × 1492 × 60 mm (height × length × thickness). The CLT panel was made of Japanese Cedar (Sugi) and classified as type Mx60-3-3, where Mx indicates a mixed-grade panel, 60 refers to the grade of the CLT laminae with a minimum modulus of elasticity (MOE) of 6.0 GPa, as specified by the Japanese Agricultural Standard (JAS) [9], and 3-3 denotes a three-layer configuration, with a total panel thickness of 60 mm, composed of three laminae, each 20 mm thick.

The RC frames were constructed and subsequently installed the CLT infill wall within it, leaving a 4mm gap between the RC frame and CLT infill, which was later filled with epoxy (E207DW). Notably, the process of inserting the CLT walls was relatively straightforward, with graduate students involved in the project managing to insert the CLT walls without requiring professional workmanship. This ease of inserting CLT infill into RC frame is a crucial point worth highlighting.

Table 1, 2, 3, and 4 show the material properties of concrete, rebar, CLT compression strength and CLT shear strength respectively, based on material tests. The values in the tables represent the mean values of three samples. The CLT tests were conducted according to the procedures mentioned in the Japanese manual [10]. The compressive strength of CLT was evaluated in the major direction (parallel to grain) and minor direction (perpendicular to grain). For specimen S-SE, tests were also conducted along the 45-degree axis. In the case of specimen S-E, tests were performed along the 30-degree, 45-degree, and 60-degree axes. These orientations were selected based on the assumed compression strut formation angles of the CLT walls in both specimens, as

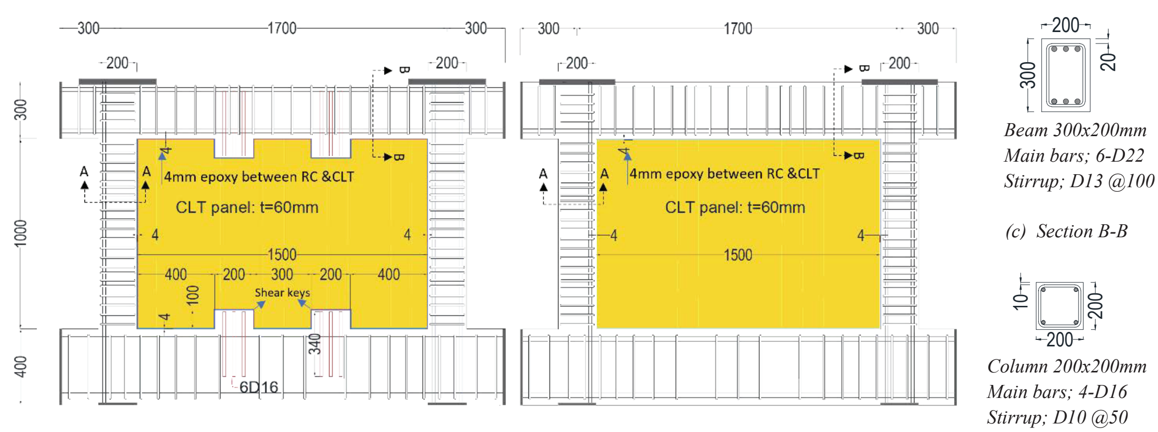

(a) Sectional elevation (S-SE) (b) Sectional elevation (S-E) (d) Section A-A

Figure. 1. Details of specimens (unit: mm) discussed later. The in-plane shear strength of the CLT was tested using four-point loading tests along the major direction. Although the tests for these materials are of the same grade and type, slight differences exist due to the specimens being loaded separately with a one-year interval and tested independently.

Table 1. Material properties of concrete

Specimen	Compressive strength (N/mm^2)	Elastic modulus (N/mm^2)
S-E	31.8	2.5×10^4
S-SE	26.3	2.1×10^4

Table 2: Reinforcement mechanical properties

Specimen	Type	Yield strength (N/mm^2)	Elastic modulus (N/mm^2)
S-E	D10(SD345)	403	1.8×10^5
	D16(SD345)	372	1.9×10^5
	D22(SD345)	363	1.8×10^5
S-SE	D10(SD345)	401	2.0×10^5
	D16(SD345)	401	1.9×10^5
	D22(SD345)	383	2.0×10^5

Table 3. Material properties of CLT compression strength

Specimen	Type	Compressive strength (N/mm^2)	Elastic modulus (N/mm^2)
S-E	Parallel to grain	21.2	6.4×10^3
	At angle 60° to grain*	5.8	2.9×10^3
	At angle 45° to grain*	6.0	2.2×10^3
	At angle 30° to grain*	6.8	1.4×10^3
	Perpendicular to grain	12.1	1.5×10^3
S-SE	Parallel to grain	23.7	6.7×10^3
	At angle 45° to grain*	5.6	1.7×10^3
	Perpendicular to grain	11.4	1.3×10^3

** The angle represents the angle between the wood grain direction in the CLT material specimen and the compression loading direction.*

Table 4. Material properties of CLT shear strength

Specimen	Shear strength (average) (N/mm^2)	Shear modulus (N/mm^2)
S-E	4.85	638
S-SE	4.23	519

2.2 Experimental setup

The specimens were tested using static cyclic loading, with the loading setup illustrated in Fig. 2. A vertical load of 400 kN (200 kN per column, assuming equal distribution) was applied to the RC columns using a single vertical hydraulic jack, corresponding to an axial stress ratio of $N / Ac / f_c \approx 0.19$, where N is the axial load (200 kN), A_c is the column's cross-sectional area, and f_c is the concrete compressive strength. The horizontal load was applied via a hydraulic jack attached to a steel beam, which was connected to the specimen through a pinned connection. To prevent torsional and out-of-plane displacement, pantographs were installed on the loading beam, ensuring that the steel beam remained horizontal.

The loading was controlled by a drift angle of R%, defined as the ratio of lateral story deformation to the story height measured at the middle depth of the beam (h = 1150 mm), as shown in Fig. 3-a).The lateral loading program consisted of 2 cycles for each peak drift angle of 0.05%, 0.1%, 0.2%, 0.4%, 0.8%, 1.6%, and 3.2%, as shown in Fig. 3.

To analyze the stress distribution in the CLT wall, triaxial strain gauges were attached to its back surface, as shown in Fig. 4. The minimum principal strain obtained from these gauges will be used to evaluate the compression strut width, which will be discussed later.

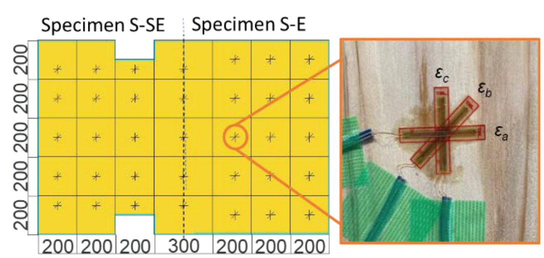

Figure 3. Triaxial strain gauges attached to the CLT wall. Unit: mm

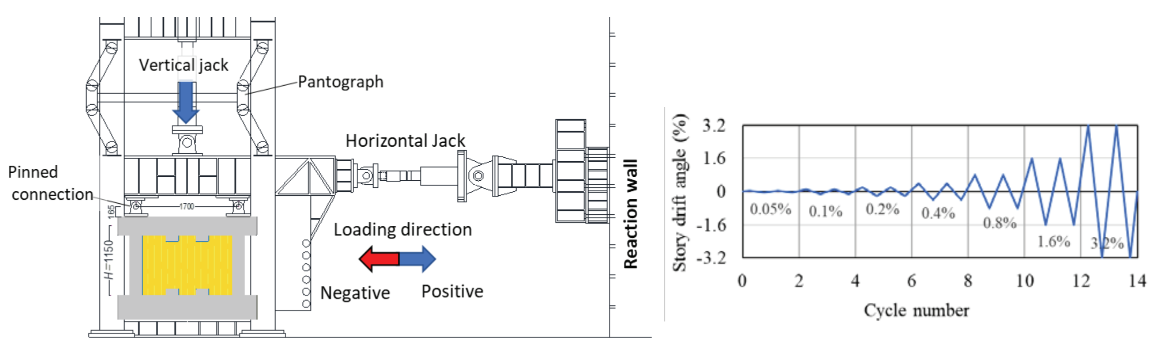

(a) Loading setup

(b) Loading protocol

Figure 2. Details of specimens (unit: mm)

https://doi.org/10.52202/080513-0105

3 – EXPERIMENTAL RESULTS

Fig. 4 and Fig. 5 show the lateral load versus story drift angle relationship for specimens S-SE and S-E, respectively. Fig. 6 a) and b) presents the crack patterns at the end of the test for specimens S-SE and S-E. Fig.6 c) and d) shows the photo of damage at story drift cycle of 3.2% at the end of the test. Fig.6 e) and f) shows the distribution of the minimum principal (compressive) strain of the CLT wall calculated from triaxial strain gauges at a story drift of 0.8%. The principal compressive strains were predominant in the diagonal direction, indicating a tendency for diagonal compression struts to form in the CLT walls. This indicates that the compression strut mechanism can be used to quantitatively evaluate the shear strength by the CLT walls which will be discussed later.

As for the failure mechanism of specimen S-SE, it is described as follows: At story drift of, R = 0.1% rad, flexural cracks emerged at the ends of the beams and at the bottom of columns. At R = 0.4% rad, shear cracks emerged in the beams. At R = 0.8% rad, the adhesion section between the CLT and RC frame, bonded by epoxy, delaminated, and small gaps appeared. Subsequently, flexural shear cracks developed at both the top and bottom of the RC columns and yielding of the main reinforcement occurred. No visible damage occurred to the CLT, except for small gaps (at epoxy region) between the RC and CLT at the corners of the frame. At R=1.6%, the main rebars yielded at the top ends (forming hinges at the bottom and top of columns), achieving the maximum lateral strength. A vertical crack emerged along the wall along the CLT's height just under the shear keys. After this point, those vertical cracks on the CLT propagated and divided the walls into three

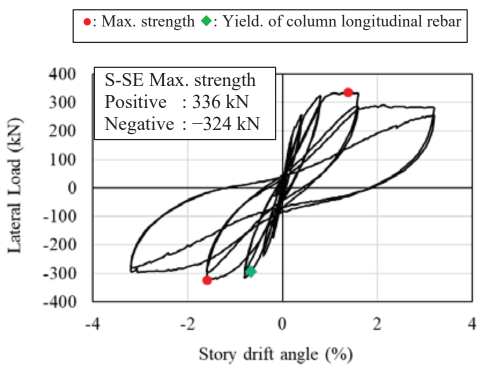

Figure 4. S-SE load-story deformation relations

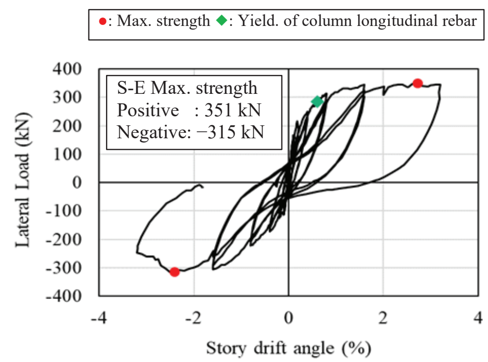

Figure 5. S-E load-story deformation relations

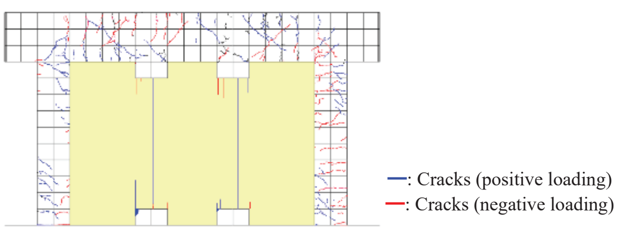

(a) Cracks observed at specimen S-SE at end of test

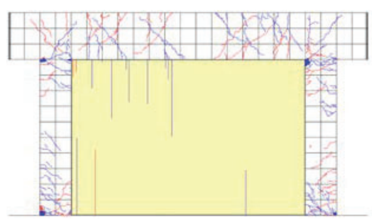

(b) Cracks observed at specimen S-E at end of test

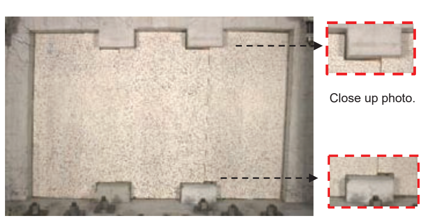

(c) Photo of specimen S-SE at end of the test

(d) Photo of specimen S-E at end of the test

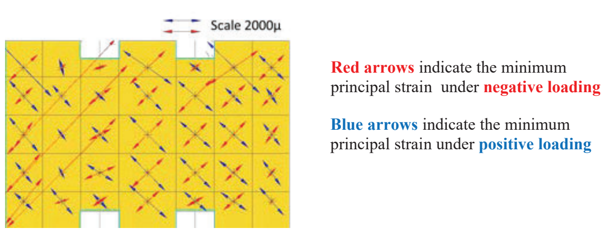

(e) Minimum principal strain of CLT in S-SE at a story drift of 0.8%.

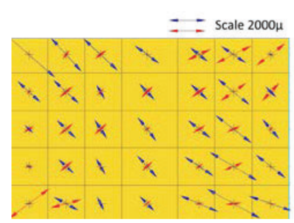

(f) Minimum principal strain of CLT in S-E at a story drift of 0.8%

Figure 6. Comparison of damage and principal strains observed for both specimens

https://doi.org/10.52202/080513-0105

panels in the middle of the shear keys and those CLT as shown in Fig. 6-c), at story drift of R= 3.2%, panels acted as rocking mechanism and the strength decreased to about 80% of the maximum strength.

As for the failure mechanism of specimens S-E is described as follows: At story drift of R = 0.1%, flexural cracks emerged at the ends of the beams and at column base. At R = 0.4%, Shear cracks emerged in the beams. At R = 0.8%, the adhesion section between the CLT and RC frame, bonded by epoxy, delaminated, and small gaps appeared. Subsequently, flexural shear cracks developed at both the top and bottom of the columns and yielding of the main reinforcement occurred. Vertical cracking occurred in the upper center of the CLT panel. At R = 2.7%, it reached the maximum strength of 351 kN (See Fig. 4). At R = 3.2%, the CLT wall began to deform out-of-plane, as shown in Fig.6-d).

A comparison between specimens S-E and S-SE shows that their lateral load capacity and stiffness were similar up to R = 0.8%. However, specimen S-SE reached its maximum strength at an earlier drift than S-E, suggesting that the shear key placement accelerated the onset of load-bearing capacity. The out-of-plane deformation occurred in S-E, but not in S-SE, indicating that the shear key placement is effective in confining CLT panel and thus avoiding the out-of-plane deformation.

4– SHEAR STRENGTH EVALUATION

As previously mentioned, the principal compressive strain of the CLT wall was predominant along its diagonal, indicating the formation of a diagonal compression strut. Based on this compressive strut mechanism, the lateral strength carried by the CLT wall was evaluated in this study. The equivalent width and inclination angle of the compressive strut was calculated based on the method proposed by Jin et al. [11].

4.1 Inclination angle of strut (strut angle)

To determine the inclination angle θ of the diagonal compression strut (hereafter referred to as the strut angle) relative to the horizontal direction, the CLT wall was divided into blocks where triaxial strain gauges were attached as shown previously in Fig.3. First, the principal compressive strain is ε_j calculated from (1) based on rosette analysis using the measurement results of triaxial strain gauges attached to the back surface of the CLT wall, and the principle compression strain angle for each block, θ_j , is determined from (2).

$$\varepsilon_j = \frac{1}{2}\left[\varepsilon_a + \varepsilon_c - \sqrt{2\{(\varepsilon_a - \varepsilon_b)^2 + (\varepsilon_b - \varepsilon_b)^2\}}\right] \tag{1}$$

$$\theta_j = \frac{1}{2}tan^{-1}\left[\frac{2\varepsilon_b - \varepsilon_a - \varepsilon_c}{\varepsilon_a - \varepsilon_c}\right] \tag{2}$$

Where:
ε_j: The principal compressive strain
θ_j: The principal compressive strain angle with respect to the horizontal direction for each block
ε_a, ε_b, ε_c: 0°, 45°, 90° direction stains (see Fig.3)
Then using the principal compressive strain measured in each block, the strut angle was calculated by averaging the weighted average of principle compression strain angle in each block. Since blocks with higher principal compressive strain were considered to have a greater influence on the strut angle, then θ was calculated as the weighted average of θ_j by ε_j as expressed in (3).

$$\theta = \left(\sum_{j=1}^{l} \varepsilon_j \times \theta_j\right) / \sum_{j=1}^{l} \varepsilon_j \tag{3}$$

Where:
l: Total number of selected measurement units (blocks)
Since the principal compressive strain forming the diagonal compression strut is distributed between 0° and 90°, only the compressive strains within these ranges were selected for each loading direction. Furthermore, only strain values below 20,000 μ, which is the measurement limit of the strain gauges used in the test, were considered valid for determining the strut angle.

Fig. 6 shows the variation of the strut angle θ at the peak of the first cycle for each loading direction. The average strut angles during positive loading were about 45° for specimen S-SE, while for specimen S-E, they were about 38°. The strut angle in specimen S-E was closer to the diagonal of the CLT wall (34°). This suggests that the shear keys in specimen S-SE influenced the strut angle of the equivalent compression strut.

4.2 Equivalent strut width

To accurately determine the equivalent width of the compression strut in the CLT wall, the rear surface of the wall—where triaxial strain gauges were installed—was divided into evenly spaced sections. These sections were oriented perpendicular to strut angle θ as shown in Fig. 7. Each section was designed to contain at least one triaxial strain gauge measurement point. The number of sections was set based on the specimen with the fewest possible divisions (S-SE), ensuring consistency across all specimens. As a result, both test specimens were divided into 9 sections.

For each section i, the arithmetic mean of the measured principal compressive strains, ε_i, was calculated and considered as the representative compressive strain for that section. Based on the measurement unit width corresponding to the selected principal compressive strain ε_j, the effective width of the compression strut for each section, $W_{e,i}$ (shown as blue arrows in Fig.7), was determined. The total equivalent width of the diagonal compression strut, W_{eq}, was calculated using (4). This equation assumes that the compression strut is uniformly distributed across the wall with an equivalent width W_{eq}.

$$W_{eq} = \left(\sum_{i=1}^{n} (\varepsilon_i \times W_{ei})\right) / \sum_{i=1}^{n} \varepsilon_i \quad (n = 9) \tag{4}$$

where ε_i: Average principal compressive strains within section i.
W_{ei}: Effective width of compression strut in section i.
n: Total number of divided sections.

Fig. 8 shows the variation in the equivalent width of the compression strut W_{eq} at the peak of the first cycle for the positive loading direction. In both specimens, W_{eq} exhibited a gradual decreasing trend. However, at R = 3.2%, the CLT wall in specimen S-E experienced

https://doi.org/10.52202/080513-0105

pronounced out-of-plane deformation, which may have affected the accuracy of W_{eq} evaluation at this point.

Additionally, the results indicate a slight difference in W_{eq} between the two specimens. Similar to the previously discussed strut angle θ, this suggests that the shear keys may have slightly influenced the compression strut resistance mechanism of the CLT wall.

4.3 Central axis of strut

To determine the position of the equivalent compression strut in the CLT wall, a reference point was set at the lower right corner for positive loading as shown in Fig.9. From this point, a reference line was drawn following the strut angle. The vertical distance from this reference line to each measured principal compressive strain was denoted as y_j.

The acting point of the compression strut (centroid), C_{yi}, for each section i was calculated by (5). This calculation accounts for the weighted average of y_j, giving greater influence to areas with higher principal compressive strain within the section.

$$Cy_i = \left(\sum_{i=1}^{m} \varepsilon_j \times y_j\right) / \sum_{i=1}^{m} \varepsilon_j \qquad (5)$$

where:
C_{yi}: centroid of the compression strut in section i
m: Number of principal compressive strains ε_j to be selected in section i
ε_j: Minimum principal compressive strain
y_j: Distance from the lower edge to the measured principal compressive strain ε_j (see Fig.9)

Next, the central axis position C_y of the equivalent compression strut was determined using (6). This calculation involved taking a weighted average of C_{yi}, giving more weight to sections with larger representative principal compressive strain ε_i. The final value of C_y represents the distance from the reference point to the central axis of the compression strut.

$$Cy = \frac{\left(\sum_{i=1}^{n} \varepsilon_i \times Cy_i\right)}{\sum_{i=1}^{n} \varepsilon_i} \qquad (n = 9) \qquad (6)$$

where:
C_y: Position of the compression strut central axis
n: Number of divided sections (n = 9)
ε_i: Average principal compressive strain in section i

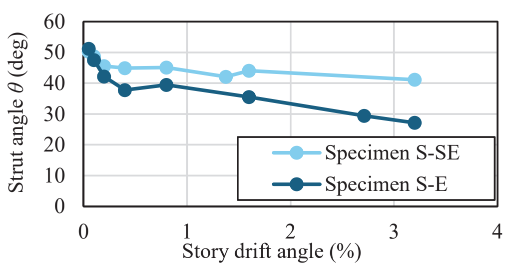

Figure 6. Strut angle θ at each story drift

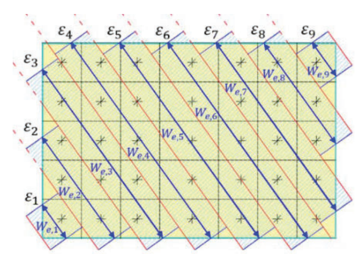

Figure 7. Method for Dividing Wall Sections and Calculating We,i

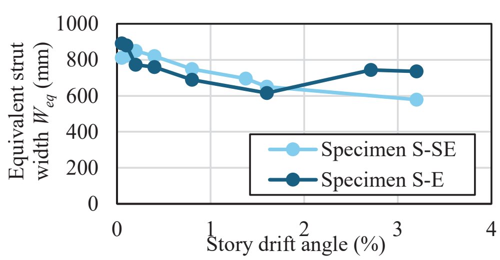

Figure 8. Compression equivalent strut at each story drift angle

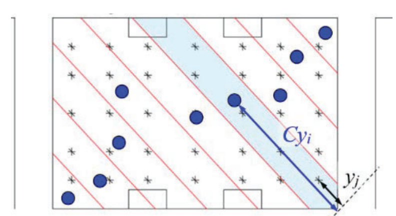

Figure 9. Simplified illustration of strut central axis Cyi

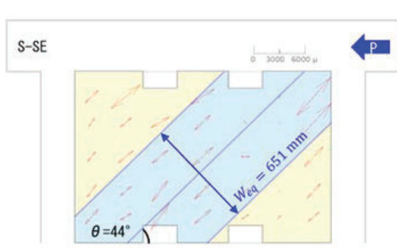

(a) Specimen S−SE

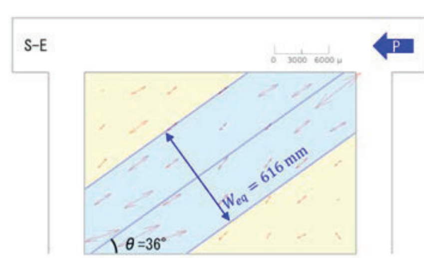

(b) Specimen S−E

Figure 10. Calculated compression equivalent strut at story drift angle of 1.6% (positive loading)

By analyzing the principal compressive strain distribution, the strut angle θ, equivalent width Weq, and central axis position C_y were determined. The results for each specimen at a story drift of R = 1.6%, where both specimens nearly reach their maximum strength, are presented in Fig. 10.

At this drift level, the equivalent strut width ranged from 0.34 to 0.36 times the diagonal length of the CLT wall for both specimens. This observation will be used in the next section to calculate the lateral strength contributed by the CLT wall.

4.4 Shear strength of strut

The lateral strength Q_w carried by the CLT wall at the maximum load-bearing capacity of each specimen could be estimated using (7), based on the compression strut mechanism.

$$Q_w = W_{eq} \times t \times \sigma_m \times cos\theta \tag{7}$$

Where:
W_{eq}: Equivalent width of the compression strut (mm)
t: thickness of the wall (= 60 mm)
σ_m: Compressive strength of CLT (N/mm²), which is taken based on the same angle of compression strut.
θ: Strut angle (illustrated in Fig. 10).

At a story drift of 1.6%, both specimens nearly reached their maximum strength, making this the reference point for evaluating their lateral strength. At this stage, the equivalent strut width, W_{eq}, was taken as 651 mm for specimen S-SE and 616 mm for specimen S-E, as shown in Fig. 10. Similarly, the strut angle, θ, was taken as 44° for specimen S-SE and 36° for specimen S-E.

The compressive strength of CLT, σ_m, at 1.6% story drift is assumed to be near its maximum compressive strength. Based on material test results in Table 3, the compressive strength for specimen S-SE was taken as 5.6 N/mm² which compressive strength at angle 45°. For specimen S-E, since the strut angle was 36°, the compressive strength was determined through linear interpolation between the values at 30° and 45°, resulting in 6.5 N/mm².

By applying these parameters, the lateral strength carried by the CLT wall, Q_{wall}, at its maximum strength is shown in Table 5.

The RC frame was designed to reach its ultimate flexural capacity, with plastic hinges forming at the ends of the columns. The lateral frame strength, Q_{fr}, was calculated using (8), and the results are presented in Table 4.

$$Q_{fr} = \frac{4M_u}{h_o} \tag{8}$$

Where M_u is the minimum plastic moment of either the column or beam calculated by [12] and h_o is the clear height of column (taken here as CLT infill height of 1000mm). The moment capacity of column ends was calculated using axial load (200kN on each column) applied by the vertical jack in the experiment.

The total lateral strength of the system was estimated by summing the lateral strength of the CLT wall (Q_w), based on the compression strut mechanism) and the lateral strength of the RC frame (Q_{fr}). These calculated values, shown in Table 4, closely match the maximum strength observed in the experimental results, validating the reliability of the analytical approach.

Table 4. Comparison of calculated and experimental values

Specimen	Q_w (kN)	Q_{fr} (kN)	***Total*** ***(Q_w+ Q_{fr})*** **(kN)**	**Experiment max. strength (kN)**
S-E	194	163	357	351
S-SE	157	167	324	336

To calculate the average shear stress of the CLT wall, the shear forces carried by the CLT (Q_w) were divided by the net cross-sectional area of the wall.

For specimen S-SE, the net cross-sectional area was found by multiplying the net panel length by the CLT thickness (60 mm). The net panel length was 1076 mm, measured at the level of the shear keys. This was determined by subtracting the 400 mm shear keys and the 4 mm epoxy injection gaps (six on each side) from the total length.

For specimen S-E, which did not have shear keys, the net panel length was 1492 mm, accounting only for the epoxy injection gaps on both sides.

Using these net cross-sectional areas, the average shear stress when the CLT wall reached its maximum strength at a story drift of 1.6% was calculated as 2.4 N/mm² for specimen S-SE and 2.2 N/mm² for specimen S-E. These values are slightly lower than the expected shear strength of CLT walls of 2.7 N/mm² calculated using the Japanese CLT Design Manual [13], and are about half of the shear strength obtained from material tests shown previously in Table 4**,** which was in the range of 4.2~4.8 N/mm².

The lower shear stress for CLT walls observed in the experimental tests suggest the need for further investigation. Possible factors include stress concentration at connections**,** epoxy injection gaps**,** CLT-RC frame interaction**,** the natural variability of the wood material and differences in loading conditions compared to standard material tests.

5–ANALYSIS MODEL

Although advanced analysis methods such as the Finite Element Method (FEM) are available, their complexity often makes them impractical for building design. For the RC+CLT system to gain wider adoption in engineering practice, simplified macro models are essential. To meet this need, a macro-model was developed.

5.1 Development of macro model

The proposed analysis model is shown in Figure 11. In this model, RC columns and beams are represented as line elements, with rotation and shear springs at their ends to capture structural deformations of the RC frame. The characteristics of these rotation and shear springs are

https://doi.org/10.52202/080513-0105

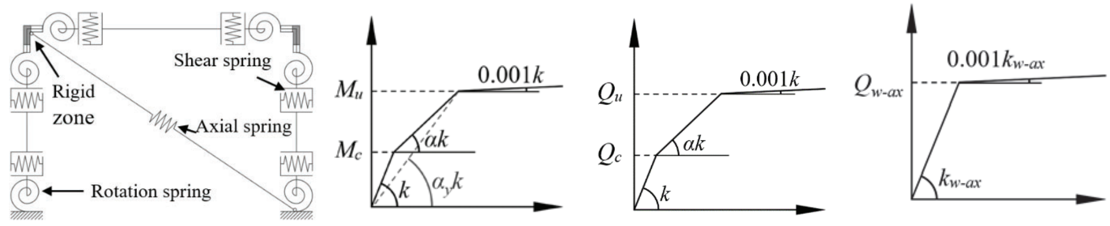

a) *Overall analysis models* b) *Rotational spring model* c) *shear spring model* d) *Axial spring model*

Figure 11. Proposed analytical model

detailed in Figures 11-b) and c). The cracking moment (M_c), ultimate moment capacity (M_u) and secant stiffness at yielding point, (a_y) (in Fig. 11b) were calculated based on [12]. The shear spring model for RC was estimated based on shear cracking strength (Q_c) and its maximum expected shear strength (Q_u) which were both calculated based on [12].

The CLT was modeled as a brace with an axial spring, similar to the idea of compression strut explained previously. The axial spring is proposed as a bilinear model as shown in Fig. 11-d). The yielding point of horizontal strength of CLT wall, Q_{wall}, was calculated by (7) (shown in previous section), considering the compression strut mechanism. The equivalent strut width and strut angle were taken based on experimental results (see Fig.10)

The initial stiffness of the CLT wall, k_w, was determined by considering shear stiffness, k_s, and rotational stiffness (rocking mechanism of CLT), k_r, as illustrated in Figure 12 and using (9)

$$k_w = \frac{1}{\frac{1}{k_s} + \frac{1}{k_r}} \tag{9}$$

Here the shear stiffness of the CLT, k_s, was calculated based on Equation (10).

$$k_s = \frac{GA}{H} = \frac{GLt}{H} \tag{10}$$

Where:
G: Elastic shear modulus of CLT wall (N/mm^2)

A: Cross-sectional area of CLT wall (mm^2)

L: Length of CLT wall (mm)

H: Height of CLT wall (mm)

The shear modulus of elasticity, G, of the CLT wall is taken based on material tests shown previously in Table 4.

The rotational (rocking) stiffness of the CLT wall, k_r, was determined based on the method proposed by Fukumoto et al. [14]. The calculated stiffness for both CLT wall specimens is summarized in Table 5.

The axial spring representing the wall was assumed to be inclined diagonally from the corners of the RC frame (as shown in Figure 11) for simplicity. Therefore, the initial stiffness k_w and the lateral strength of the CLT wall Q_w were transformed into equivalent values in the direction of the axial compressive spring strength in the analytical model using (11) and (12):

$$Q_{w-ax} = Q_w / \cos\theta_{sp} \tag{11}$$

$$k_{w-ax} = k_w / \cos^2\theta_{sp} \tag{12}$$

Where $\theta_{sp} = 34°$ represents the strut angle of the axial spring.

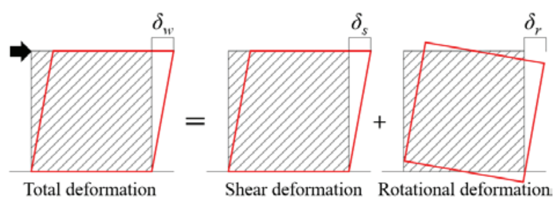

Fig. 12. Illustration of the main deformation considered for CLT walls infilled in RC frame

Table 5. Calculated stiffness for the CLT wall

Specimen	k_s	k_r (kN/mm)	k_w (kN/mm)
S-E	57.6	239.9	46.4
S-SE	45.1	248.3	38.2

5.2 Analytical results

A pushover analysis was conducted using the developed macro-model, and the results were compared to the experimental findings in Fig. 14 and 15. The analysis included two cases: (1) the full hybrid system, where the CLT wall was modeled as an axial spring representing the diagonal compression strut, and (2) the bare RC frame, where the CLT panel contribution was removed for comparison.

In general, the analytical model successfully captured the key trends in stiffness degradation, yielding, and peak strength for both specimens. The initial lateral stiffness predicted by the model was slightly lower than the experimental values, likely due to simplifications in the representation of connection flexibility and bi-linear model used for the CLT panels.

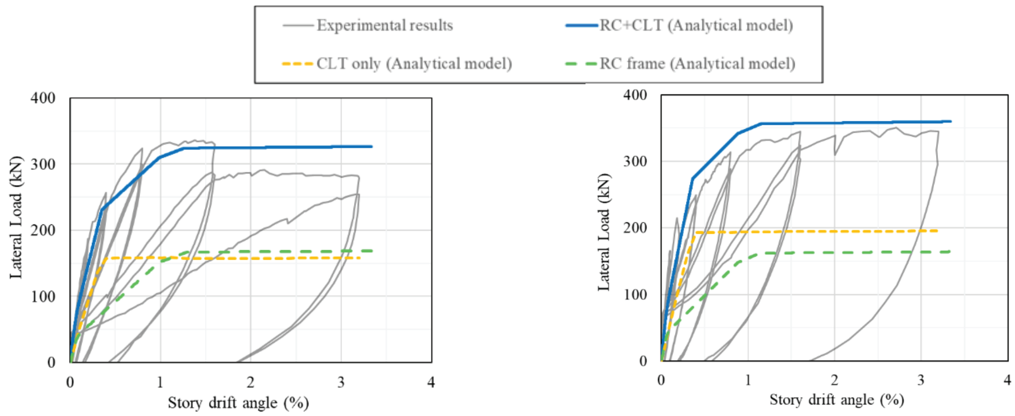

a) Specimen S-SE *b) Specimen S-E*

Fig. 14. Comparison of analytical and experimental results

The stiffness degradation trend was well simulated, particularly up to the drift ratio at which plastic hinge formation was observed in the columns. The predicted peak lateral strength closely matched the experimental results, with differences of less than 5% for both specimens.

The model did not incorporate post-peak softening behavior, leading to deviations between the analytical and experimental results beyond a drift ratio of 2%. Further studies are needed to incorporate post-peak strength degradation.

6 – CONCLUSION

This study investigated the seismic performance of hybrid (RC) frames with (CLT) shear walls through experimental testing and analytical modelling. Two 1/3-scale specimens were subjected to cyclic lateral loading to examine the effect of different connection systems, one utilizing shear keys (S-SE) and the other relying solely on epoxy bonding (S-E). The following are the main findings:

- The maximum lateral strength was 351 kN for Specimen S-E and 336 kN for Specimen S-SE, showing less than a 5% difference. Both specimens exhibited similar lateral stiffness up to 0.8% drift, beyond which slight differences occurred. Specimen S-SE reached peak strength at 1.6% drift, while Specimen S-E continued strengthening until 2.7% drift, suggesting minor effects of shear keys on force transfer. Specimen S-E experienced out-of-plane deformation beyond 3.2% drift. On the other hand, the shear keys in S-SE effectively confined the CLT panel against out-of-plane failure, improving stability. However, as for S-SE, vertical cracks occurs along the CLT wall just under the shear keys, which results in splitting the shear walls beyond 1.6% story drift.

- The results confirmed that CLT infill contributed to the lateral load capacity and worked effectively as shear walls. The analysis using data of strain gauges and calculation of principal compression strain, showed that diagonal compression strut mechanism governing shear transfer. The diagonal compression strut width was 0.34 times the diagonal length in Specimen S-SE and 0.36 times in Specimen S-E, indicating a minor influence of the shear keys on strut formation.

- The measured shear stress was 2.4 N/mm² (S-SE) and 2.2 N/mm² (S-E), significantly lower than the 4.2–4.8 N/mm² as expected from material tests. This reduction could be attributed to stress concentrations at connections and bidirectional loading effects which is different to the loading condition in material test standards. The presence of shear keys had minimal impact on the overall shear contribution.

- The developed macro-model closely matched experimental results, effectively capturing stiffness degradation and peak strength. The model did not incorporate post-peak softening behavior, and the ultimate deformation capacity was not fully captured, leading to deviations between the analytical and experimental results beyond a drift ratio of 2%.

Future studies will focus on optimizing connection details and refining analytical models to account for strength degradation beyond the peak load. Additionally, long-term durability concerns, including creep in CLT, shrinkage/swelling of CLT, and the degradation of epoxy adhesive between RC and CLT, require further investigation.

7 – REFERENCES

[1] Maeda, M., Al-Washali, H. A., Takahashi, K., & Suzuki, K. (2011). Damage to reinforced concrete school buildings in Miyagi after the 2011 Great East Japan Earthquake. In Proceedings of the International Symposium on Engineering Lessons Learned from the (pp. 1120-1131).

[2] Marquis, F., Kim, J. J., Elwood, K. J., & Chang, S. E. (2017). Understanding post-earthquake decisions on multi-storey concrete buildings in Christchurch, New Zealand. Bulletin of earthquake engineering, 15, 731-758.

https://doi.org/10.52202/080513-0105

[3] Alwashali, H., Islam, M. S., Sen, D., Monical, J., & Maeda, M. (2020). Seismic capacity of RC frame buildings with masonry infill damaged by past earthquakes. Bulletin of the New Zealand Society for Earthquake Engineering, 53(1), 13-21.

[4] Haba, R., Kitamori, A., Mori, T., Fukuhara, T., Kurihara, T., & Isoda, H. (2016). Development of clt panels bond-in method for seismic retrofitting of RC frame structure. J. Struct. Constr. Eng, 81, 1299-1308.

[5] Stazi, F., Serpilli, M., Maracchini, G., & Pavone, A. (2019). An experimental and numerical study on CLT panels used as infill shear walls for RC buildings retrofit. Construction and building materials, 211, 605-616.

[6] Smiroldo, F., Kallioras, S., Sommacal, G., Bournas, D., Piazza, M., & Giongo, I. (2023). Full-scale testing of masonry-infilled RC frames retrofitted with cross-laminated timber panels. Engineering Structures, 294, 116789.

[7] Too, R. Y. J., Sakashita, M., Isoda, H., & Araki, Y. (2024). Seismic performance of RC frame structures with infill CLT shear walls. Engineering Structures, 303, 117473.

[8] Alwashali, H., Aljuhmani A. (2023). Study on failure mechanisms of hybrid structure of reinforced concrete frame with CLT infill. World Conference on Timber Engineering (WCTE 2023)

[9] Ministry of Agriculture, Forestry and Fisheries. Japanese Agricultural Standard for Cross Laminated Timber (JAS 3079). Japan: MAFF, 2019. https://clta.jp/wp-content/uploads/2019/08/JAS3079-2019_CLT.pdf.

[10] Japan Housing and Wood Technology Center. HOWTEC Structural Wood Strength Test Manual. 2011.

[11] Jin, K., Choi, H., Nakano Y. (2016) Experimental Study on Lateral Strength Evaluation of Unreinforced Masonry-Infilled RC Frame, Vol.32, No.3, Earthquake Spectra, pp1725-1747

[12] Architectural Institute of Japan (AIJ) (2016). AIJ standard for lateral load-carrying capacity calculation of reinforced concrete structures. (in Japanese)

[13] Japan Housing and Wood Technology Center, Design and Construction Manual for CLT Buildings, Tokyo, Japan, 2016. (in Japanese).

[14] Fukumoto, K., & Isoda, H. (2021). Study on compressive stress transfer in joints of steel frame hybrid structure with CLT infill shear walls. Journal of Structural and Construction Engineering, 86(788), 1440–1451.